Influence of hydrated lime on the surface properties and interaction of kaolinite particles

4 AUTHORS, INCLUDING:

Yadeta C. Chemeda
Institut Français des Sciences et Technolog…

2 PUBLICATIONS **1** CITATION

SEE PROFILE

Dimitri Deneele
IFSTTAR/IMN

25 PUBLICATIONS **168** CITATIONS

SEE PROFILE

G.E. Christidis
Technical University of Crete

48 PUBLICATIONS **690** CITATIONS

SEE PROFILE

Research Paper

Influence of hydrated lime on the surface properties and interaction of kaolinite particles

Yadeta C. Chemeda [a,b], Dimitri Deneele [a,b,*], George E. Christidis [c], Guy Ouvrard [b]

[a] LUNAM, IFSTTAR, Institut Français des Sciences et des Technologies des Transports, de l'Aménagement et des Réseaux, BP 4129, route de Bouaye, 44332 Bouguenais, France
[b] Institut des Matériaux Jean Rouxel (IMN), Université de Nantes, CNRS, 2 rue de la Houssinière, BP 32229, 44322 Nantes Cedex 3, France
[c] Technical University of Crete, Department of Mineral Resources Engineering, 73100 Chania, Greece

ARTICLE INFO

ABSTRACT

Lime is a widely used chemical additive in the stabilization of problematic soils. However, the physico-chemical mechanism involved, particularly in the short-term, is still not fully understood. In the present work, the influence of hydrated lime ($Ca(OH)_2$) on the rheological properties of kaolinite dispersion has been investigated. The influence of the type of cation and pH on the interfacial chemistry and particle interaction were also examined. The result showed that kaolinite predominantly adsorbs Ca^{2+} and $CaOH^+$ at pH = 7 and pH = 12.6 respectively. With increasing concentration of $Ca(OH)_2$, the value of storage modulus (G'), Bingham yield stress (τ_B) and cohesive energy density (Ec) initially decreased at lower concentration (≤ 5.5 mmol/l) followed by increase at higher concentration (≥ 11 mmol/l); in contrast these parameters decreased monotonously with increasing the concentration of NaOH. The strain hardening characteristic of loss modulus (G'') curve was found to be very sensitive to change in surface chemistry and the associated particle organization. The modification in the mechanical properties of the kaolinite with varying amount of $Ca(OH)_2$ was attributed to the aggregation microstructure of kaolinite particles. The Ca-ion at higher pH promotes linkage between particles and provides the most efficient way to form dense, tightly packed flocs, which behave as individual coarse grained materials (silt or sand).

© 2015 Elsevier B.V. All rights reserved.

1. Introduction

The soft soils that are usually encountered in construction sites are generally unsuitable for construction works due to their weak mechanical properties and poor workability. Besides, clayey soils exhibit volume change in response to seasonal moisture variation which influences the performance and life time of shallow founded and light weighted structures such as pavements. On the other hand, re-using these materials after stabilization is vital to minimize the cost and environmental impact of construction works. The stabilization of the problematic soils is commonly achieved by mixing them with water and lime or Portland cement and has been thoroughly studied for a long time (Diamond and Kinter, 1965; Choquette et al., 1987; Locat et al., 1990; Verhasselt, 1990; Bell, 1996; Al-Mukhtar et al., 2010; Kavak and Baykal, 2012; Pomakhina et al., 2012; Eisazadeh et al., 2012).

Most of the previous studies cited above refer mainly to the long-term effect of lime on soil property. The physico-chemical mechanism

involved in long-term, i.e. pozzolanic reaction is well understood. In contrast, the mechanism involved in short-term, particularly an increase in unconfined compressive strength (UCS) and shear strength of clayey soil prior to the precipitation of secondary phases (CSH and/or CASH), has not been fully evaluated. This has usually been explained by the reduction of the thickness of diffuse double layer (DDL) around clay mineral particles in the presence of Ca-ion. However, $CaCl_2$ solution, with similar calcium concentration ($[Ca^{2+}] = 22$ mmol/l) to that of the saturated lime solution, has no significant effect on mechanical property of expansive clayey materials (Diamond and Kinter, 1965; Verhasselt, 1990). Therefore, the cation exchange reaction and compression of the DDL alone cannot explain the short-term improvement in the mechanical properties of lime treated clayey soil. Understanding the reaction mechanism in short-term is important if one want to optimize the lime treatment technique. In addition, the short-term reaction (first minute up to 24 h after mixing) is a crucial stage as it determines the long-term characteristics (durability and mechanical characteristic) of treated material (Konan et al., 2009).

Surface chemistry determines the interaction between dispersed clay mineral particles (i.e. attractive or repulsive) and affects their probable orientation with respect to each other (Van Olphen, 1964; Kretzschmar et al., 1998; Johnson et al., 1998; Abend and Lagaly, 2000; Penner and Lagaly, 2001; Tombacz and Szekeres, 2004, 2006).

* Corresponding author. Fax: +33 240845997.
E-mail addresses: yadeta.chemeda@cnrs-imn.fr (Y.C. Chemeda), Dimitri.Deneele@ifsttar.fr (D. Deneele), christid@mred.tuc.gr (G.E. Christidis), Guy.Ouvrard@cnrs-imn.fr (G. Ouvrard).

On the other hand, since the magnitude and direction of the inter-particle forces depend on the separation distance and surface area over which the interaction occurs (Van Olphen, 1964), particle orientation in turn may affect the magnitude of inter-particle cohesive forces and mechanical strength of the aggregated flocs. It is commonly observed that the mode of interactions and resulted floc structures are affected by different parameters such as the ionic strength and pH of the medium (Abend and Lagaly, 2000; Penner and Lagaly, 2001; Tombacz and Szekeres, 2004, 2006; Gupta et al., 2011). Furthermore, pH was indicated to play a role in the hydrolysis reaction of multivalent cation (Mpofu et al., 2003). This is expected to take place during lime addition, since it modifies both the concentration of calcium and pH of the dispersion. Thus, the interfacial chemistry of clay mineral particles and the interaction between them in calcium rich alkaline condition are central in understanding the causes of short-term improvement of the mechanical properties of lime treated clayey soils. In other words, the knowledge of clay mineral particle interactions in the presence of Ca and OH^- ions is important.

The rheological behavior of colloidal particles is closely related to the dispersion microstructure at rest and under stress. Consequently, many workers have used rheological techniques to indirectly assess the physicochemical force between colloidal particles and the associated aggregation structure (Johnson et al., 1998; Abend and Lagaly, 2000; Hyun et al., 2002; Mpofu et al., 2003; Tombacz and Szekeres, 2004, 2006; Bossard et al., 2007; Shankar et al., 2010; Chemeda et al., 2014). Although the effect of ionic strength and pH on the rheological properties of clay mineral dispersion has been thoroughly studied (Abend and Lagaly, 2000; Duran et al., 2000; Ramos-Tejada et al., 2001; Nasser and James, 2006, 2008; Tombacz and Szekeres, 2004, 2006), a detail description of particle interaction in calcium rich alkaline condition such as in lime solution is rarely presented in the literature. The limited information is considered important, since in addition to determining the aggregation structure and mechanical strength of flocs, it can influence the mixing ability of the soil with the lime solution and affects the long-term reaction.

In the present work, the rheological behavior as a function of hydrated lime was investigated to better understand the role of Ca^{2+} and OH^- ions in the modification of surface property and interaction of kaolinite (Kaol) particles. Furthermore, the influence of cation type (Ca^{2+} vs. Na^+) and pH ($Ca(OH)_2$ vs. $CaCl_2$) was also studied. The interfacial chemistry was assessed via calcium adsorption and zeta potential measurements. The size of the aggregated particle structure was estimated using dynamic light scattering (DLS) in order to demonstrate further the particle interaction and flocs formed at different conditions. Finally, the particle aggregation mechanism with varying amount of $Ca(OH)_2$ is proposed.

2. Materials and methods

2.1. Materials and characterization

Two Kaol samples, KGa-1b (low-defect) and KGa-2 (high-defect) purchased from the Source Clay Repository of the Clay Minerals Society, were used after de-carbonation and Na^+-homoionization based on the following procedure: carbonates were dissolved at pH = 5 and 80 °C in sodium acetate–acetic acid buffer and Na^+-homoionization was obtained by three times sodium exchange in 1M NaCl solution followed by several washing and centrifugation cycles until the supernatant was chloride free (silver nitrate test) and had conductivity below 5 μS/cm. Bulk mineralogy of the samples was determined by X-ray powder diffraction (XRD), on randomly oriented samples, with a Brucker AXS D8 device, using CuKα (λ = 0.154 nm) radiation and a step size of 0.021 °2θ. Both samples consist of Kaol (>97 mass%) quartz and anatase (<3 mass% in total). The SEM micrographs confirm the pseudo-hexagonal shape and platy features of the Kaol particles in the two samples (Fig. 1).
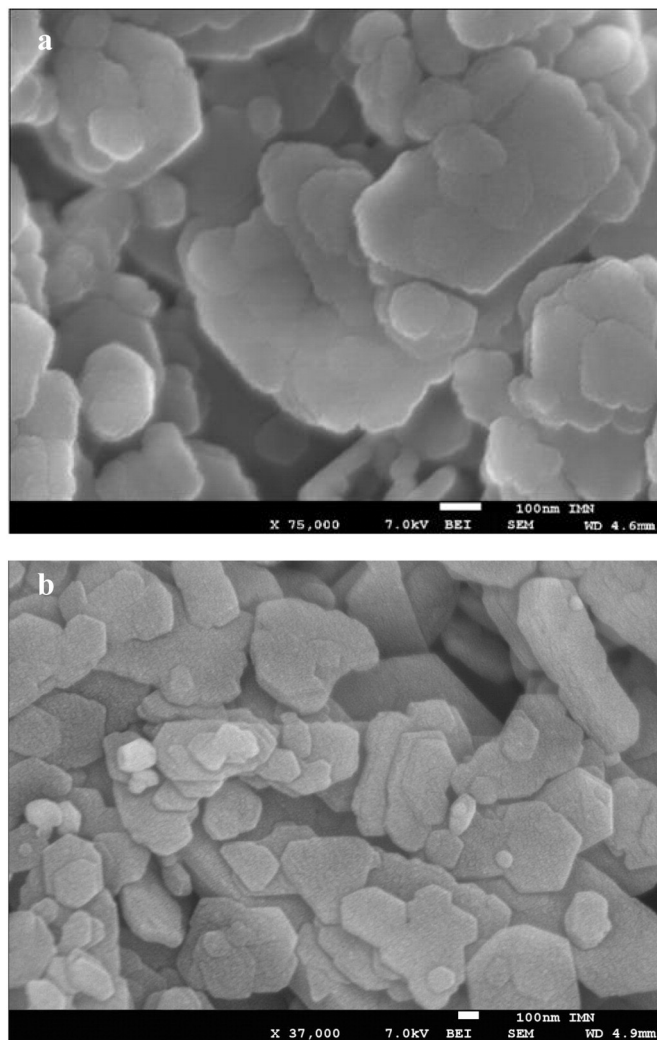

Fig. 1. SEM image of a) high defect, KGa 2 and b) low defect, KGa-1b Kaol.

The thickness of aggregated particles of the well-crystallized Kaol (KGa-1b) is higher than the poorly crystallized Kaol (KGa-2). The specific surface area, determined by nitrogen adsorption (BET method), was 9.95 and 18.6 ± 0.1 m²/g for KGa-1b and KGa-2, respectively suggesting that KGa-2 Kaol contains finer particles.

2.2. Zeta potential and size measurement

Electrophoretic mobility measurement was performed at 20 °C in a capillary cell with Malvern Nano Zetasizer apparatus and the Smoluchowski's equation was utilized to convert electrophoretic mobility to zeta potential. The measurements were carried out on agitated dispersions of Kaol particles (100 mg/l) dispersed in 10 mM NaCl solution. The pH of the dispersions was adjusted between 1 and 13 by adding either HCl, NaOH or $Ca(OH)_2$ solutions, equilibrated by agitation for 24 h in carbon dioxide free environment, and the pH was measured directly before introducing sample in to the capillary cell. Dynamic light scattering (DLS) measurements were performed at 20 °C and laser scattering at 173° to monitor the evolution of average particle size under different conditions (0 mmol/l, 22 mmol/l NaOH and 22 mmol/l $Ca(OH)_2$). For this purpose, the <1 μm fractions of Kaol particles were extracted by dispersing about 10 g of sample in 1 L ultra-pure water followed by centrifugation.

2.3. Adsorption experiments

The Kaol samples were first homo-ionized by Na^+ at pH 7. Then, the samples (6 g) were kept in contact with 30 ml freshly prepared saturated lime solutions ($[Ca^{2+}]_0 = 22$ mmol/L and initial pH 12.6) and $CaCl_2$ solution ($[Ca^{2+}]_0 = 22$ mmol/L and initial pH 7) in centrifuge tubes and were mechanically shacked for 5 min and centrifuged for 15 min at 8000 rpm. The supernatant was subsequently collected for measurement of Ca^+ and Na^+ concentrations with inductively coupled plasma-optical emission spectroscopy (ICP-OES). A lower contact time (20 min) was applied in this experiment to minimize the risk of dissolution of Kaol particles in alkaline conditions. The amounts of Ca^{2+} and OH^- adsorbed and Na^+ desorbed were determined in moles of ions per gram of clay mineral using mass balance equation as follows:

$$q = V_0 \left(\frac{C_i - C_f}{M} \right) \qquad (1)$$

where C_i represents concentration of ions (Ca^{2+}, Na^+ and OH^-) in the initial solution, C_f is the concentration of ions in separated supernatant, V_0 is the initial volume of the lime solution (30 ml) and M is the mass of the Kaol (6 g).

2.4. Rheometry

All the Kaol dispersions were prepared by dispersing appropriate amount of Kaol powder in solution with different concentrations of $Ca(OH)_2$ solution and then well mixed and ultrasonified for 5 min to disintegrate clay mineral aggregates and obtain homogeneous dispersions. Subsequently, they were sealed to prevent evaporation and left to age overnight in a glove box. After aging, the dispersions were stirred and ultrasonified for 5 min immediately before determination of the rheological properties. The rheological measurements were performed at controlled temperature (20 °C), with a plate–plate rotating rheometer (Anton Par MCR 10, with plate diameter of 50 mm and gap fixed to 1 mm) which allowed stress or strain controlled experiments. Since the structure of Kaol dispersions is sensitive to shear history during loading, which thus may affect measurements, after loading in the rheometer and pre-shearing, the samples were kept at rest for 3 min before starting the measurements. The resting time (time needed for the gel structure to rebuild) has been first determined from oscillatory measurement performed in the linear viscoelastic domain. Briefly, immediately after loading the sample and pre-shearing, the time evolution of storage modulus (G′) at a frequency of 1 Hz is followed and the time needed to attain a G′ constant value is determined. This time, which is about 3 min, is considered as the time needed for the stabilization of internal network structure. Three types of rheological measurements were performed sequentially on the same dispersion (oscillatory (strain and frequency sweep) → creep–recovery → flow curve) with 3 min pause between them. This sequence is followed because the deformation in the former cases (oscillatory and creep–recovery measurement) is lower than the flow curve measurement. To assure the reproducibility of the results, the measurements were repeated in triplicate for each experiment by changing the dispersion, and the average value is presented.

2.4.1. Dynamic (oscillatory) measurements

This technique concerns the response of the material to an oscillating stress or strain (i.e. by applying a sinusoidal input strain and recording the subsequent sinusoidal shear stress) (Tadros, 1996). Two types of oscillatory experiments were carried out: strain and frequency sweep. In the frequency sweep experiment, the strain or stress was kept constant in the linear viscoelastic region, where the moduli are independent of the applied strain, and storage modulus (G′) and loss modulus (G″) were measured as a function of frequency (0.5–5 Hz). This experiment shows how the viscous and elastic behavior of the material changes with rate of application of strain and stress. In the amplitude sweep experiment G′ and G″ were measured as a function of strain amplitude at constant frequency. A typical shear amplitude dependence of the G′ and G″ of the Kaol dispersions at the frequency of 1 Hz is shown in Fig. 2. With the exception of Kaol dispersions in $CaCl_2$ solution, this viscoelastic behavior is representative of those obtained for the viscoelastic Kaol dispersions. Three regions were identified: linear viscoelastic region, non-linear viscoelastic region and viscouse region. Only the first two regions (semi-solid dispersion) were considered in this study to examine the interaction of Kaol particles under different concentrations of $Ca(OH)_2$ solution. The linear viscoelastic limit is marked at strain amplitude (γ_{cr}) where further increase in strain amplitude caused G′ and G″ to gradually decrease and increase, respectively.

2.4.2. Creep–recovery

In this experiment, a constant stress in the linear viscoelastic region (≤ 1 Pa) was applied on the system, which was placed in the gap between the two parallel plates of the rheometer, and the strain (relative deformation) was monitored as a function of time for a period of 1 min. At t = 1 min, the stress was removed and the relative deformation was followed for another 1 min. The compliance (J) at any time is related with deformation (γ) by Eq. (2).

$$J(t) = \gamma(t)/\sigma \qquad (2)$$

2.4.3. Steady state flow curves

Flow curves of Kaol dispersions with different solid contents were obtained in the shear rate range 0–100 s^{-1}, with 50 linearly spaced steps. To examine the interaction between Kaol particles, once the curve of shear stress versus shear rate was obtained under the given experimental conditions, the value of the extended yield stress or Bingham yield stress (τ_B) was determined from the intersection of the extrapolated linear portion of the flow curve with the stress axis. The method of least squares ($r^2 > 0.98$) was used to determine the intersection.
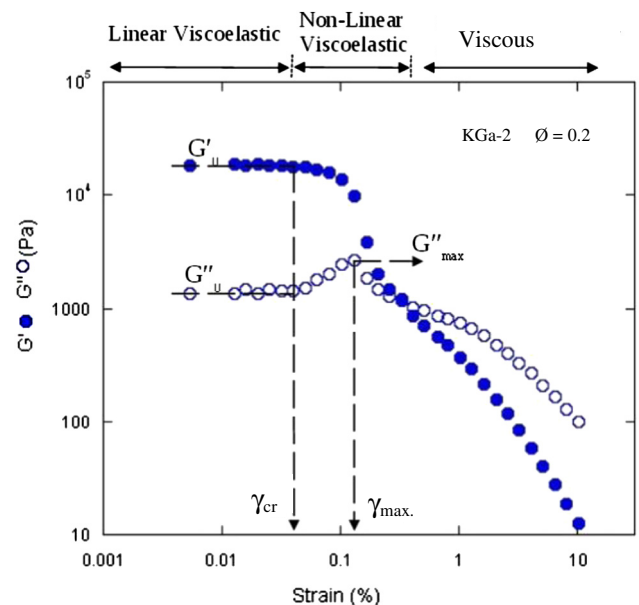

Fig. 2. The typical curve of storage modulus (G′) and loss modulus (G″) as a function of strain amplitude (at frequency of 1 Hz).

3. Result and discussion

3.1. Kaol–lime solution interfacial chemistry

3.1.1. Zeta potential

The zeta potential of 100 mg/l Kaol dispersions at 0.01 M NaCl background electrolyte as a function of pH is presented in Fig. 3. At lower pH, the response of the zeta potential to pH change depends on the surface properties of Kaol i.e. the rate of the change is higher for high defect Kaol (KGa-2) than for low defect Kaol (KGa-1b). At higher pH, the zeta potential becomes more negative with increasing amount of NaOH, signifying a more prominent influence of silanol and aluminol functional groups at the crystal edges and possibly on the octahedral basal face. In dispersions where pH was adjusted by $Ca(OH)_2$ addition, a strong decrease of the magnitude of the zeta potential was observed at pH > 9, accompanied by a negative to positive charge reversal. Unlike the lower pH region, no significant difference was observed between the dispersions of the two Kaol both in the presence of NaOH and $Ca(OH)_2$, suggesting that the zeta potential of the Kaol particles at higher pH is largely controlled by the nature of the cation (i.e. hydrolysable or not). The adsorption of the first hydrolysis product of Ca ($CaOH^+$), which starts to form at pH ≥ 10 (Mpofu et al., 2003, 2005), is reported to be the main cause for negative to positive charge reversal. Similar hydrolysable metal ion–mineral particle zeta potential behavior has been reported in other studies (James and Healy, 1972; Atesok et al., 1988; Mpofu et al., 2003, 2005).

3.1.2. Calcium adsorption

The comparison of charge of Kaol calculated from desorbed sodium (i.e., permanent charge site) and adsorbed calcium (i.e., total charge site) at pH 7 ($CaCl_2$ solution, $[Ca^{2+}]_0 = 22$ mmol/L) and pH 12.6 ($Ca(OH)_2$ solution, $[Ca^{2+}]_0 = 22$ mmol/L) is shown in Table 1. It is apparent that the charges estimated from both desorbed sodium and adsorbed calcium are comparable in the case of $CaCl_2$ solution suggesting that the adsorption of Ca-ion predominantly takes place on the permanent charge and $Si-O^-$ sites. In contrast, the total charge estimated from adsorbed calcium is at least four times higher than the charge estimated from desorbed sodium in the case of $Ca(OH)_2$ solution suggesting that more pH dependent charge sites were created in alkaline condition most likely on the edges ($Al-O^-$) and at octahedral faces.
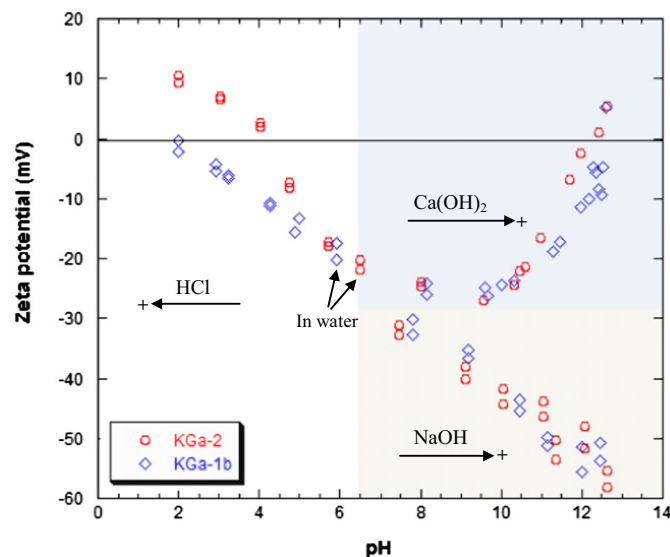

Fig. 3. Zeta potential of Kaol dispersions (100 mg/l, 0.01 M NaCl) as a function of pH adjusted with addition of HCl, NaOH and $Ca(OH)_2$.

Table 1
Comparison of charge (meq/100 g) estimated from desorbed sodium and adsorbed calcium in the case of $CaCl_2$ and $Ca(OH)_2$ solution. Initial concentration of calcium in both solutions is 22 mmol/l.

	$CaCl_2$ (pH = 7)		$Ca(OH)_2$ (pH = 12.6)	
	Na	Ca	Na	Ca
KGa-2	1.2	2.2	1.1	12.8
KGa-1b	1.4	2	1.3	8.1

An attempt was also made to identify the species of calcium adsorbed on Kaol a) using the ratio of sodium desorbed to calcium adsorbed and b) from the ratio of the hydroxyl to calcium adsorbed (Table 2). In the case of $Ca(OH)_2$ solution, the Na/Ca ratio in both samples is lower than 1 indicating the adsorption of calcium ion was controlled by a combination of adsorption of $CaOH^+$ on permanent charge site (Na/Ca = 1) and adsorption of calcium ion by mechanism that did not involve the release of sodium ion (Na/Ca = 0) such as precipitation of $Ca(OH)_2$ and adsorption on non-permanent charge sites. The OH/Ca ratio, which is higher than 1, also represents a combination of adsorption of $CaOH^+$ (OH/Ca = 1) and precipitation of $Ca(OH)_2$ (OH/Ca = 2). However, since precipitation is a slow process, it might not be a plausible calcium uptake mechanism in the current experimental conditions (<20 min contact time), rendering adsorption of $CaOH^+$ on non-permanent charge sites the possible reason for excess Ca-adsorption. In addition, hydroxyls were also consumed in the dissociation of OH functional groups ($Al-OH + OH^- \rightarrow Al-O^- + H_2O$) raising the OH/Ca ratio. Hence, the OH/Ca (OH adsorbed with Ca) ratio is expected to be lower than that included in Table 2. Therefore, the most likely adsorbed species of Ca from $Ca(OH)_2$ solution is $Ca(OH)^+$ both on permanent and pH dependent charge sites.

This is verified by the fact that the sum of the amount of Na-ions desorbed, which represents the amount of Ca adsorbed on permanent charge sites, and the amount of excess adsorbed OH-ions (N°OH– N°Ca), which represents the number of new charge (pH dependent) sites generated for Ca adsorption by the dissociation of functional groups, is equal to the amount of Ca-ions adsorbed (Table 3).

In the case of $CaCl_2$ solution, although the Na/Ca ratio is lower than 2, it is expected to be higher than the value listed in Table 2, because the charge estimated from the adsorbed calcium is slightly higher than that of desorbed sodium (Table 1). This suggests that Ca^{2+} is the adsorbed species from $CaCl_2$ solution at pH 7. These data are in full accordance with the pH dependent hydrolysis and fractional abundance of different species of Ca(II) (Mpofu et al., 2003, 2005), which reports that, the fractional abundance of the first hydrolysis product ($CaOH^+$), which forms at pH > 10.5, increases dramatically at pH between 10.5 and 14, while Ca^{2+} is the dominant species of Ca(II) at lower pH. Based on these facts, the following ion exchange mechanisms from the two solutions are proposed:
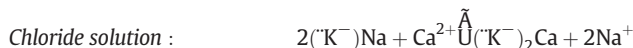
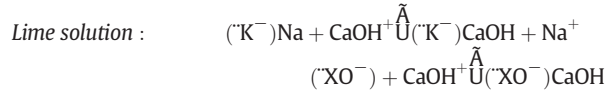$$\text{Chloride solution}: \qquad 2(¨K^-)Na + Ca^{2+} Ũ (¨K^-)_2Ca + 2Na^+$$

Table 2
Ratio of amount of Na desorbed to Ca adsorbed and number of OH adsorbed to Ca adsorbed.

	$CaCl_2$ (pH = 7)		$Ca(OH)_2$ (pH = 12.6)	
	Na/Ca	OH/Ca	Na/Ca	OH/Ca
KGa-2	1.3	–	0.2	1.8
KGa-1b	1.4	–	0.3	1.7

Table 3
The amount of sodium desorbed, calcium adsorbed, hydroxide ion adsorbed and the number of hydroxide adsorbed minus calcium adsorbed from lime solution ([Ca] ≈ 22 mmol/l and pH = 12.6).

Number (μmol/g of clay mineral)				
	Na	Ca	OH	OH–Ca
Kga-1b	13	40	70	30
Kga-2	12	64	116	52

Lime solution : $(¨K^-)Na + CaOH^+ \overset{\tilde{A}}{U} (¨K^-)CaOH + Na^+$

$(¨XO^-) + CaOH^+ \overset{\tilde{A}}{U} (¨XO^-)CaOH$

where $\equiv K^-$ and $\equiv XO^-$ represent a permanent charge site (on tetrahedral basal face) and a pH dependent charge site (on lateral face and octahedral basal face), respectively.
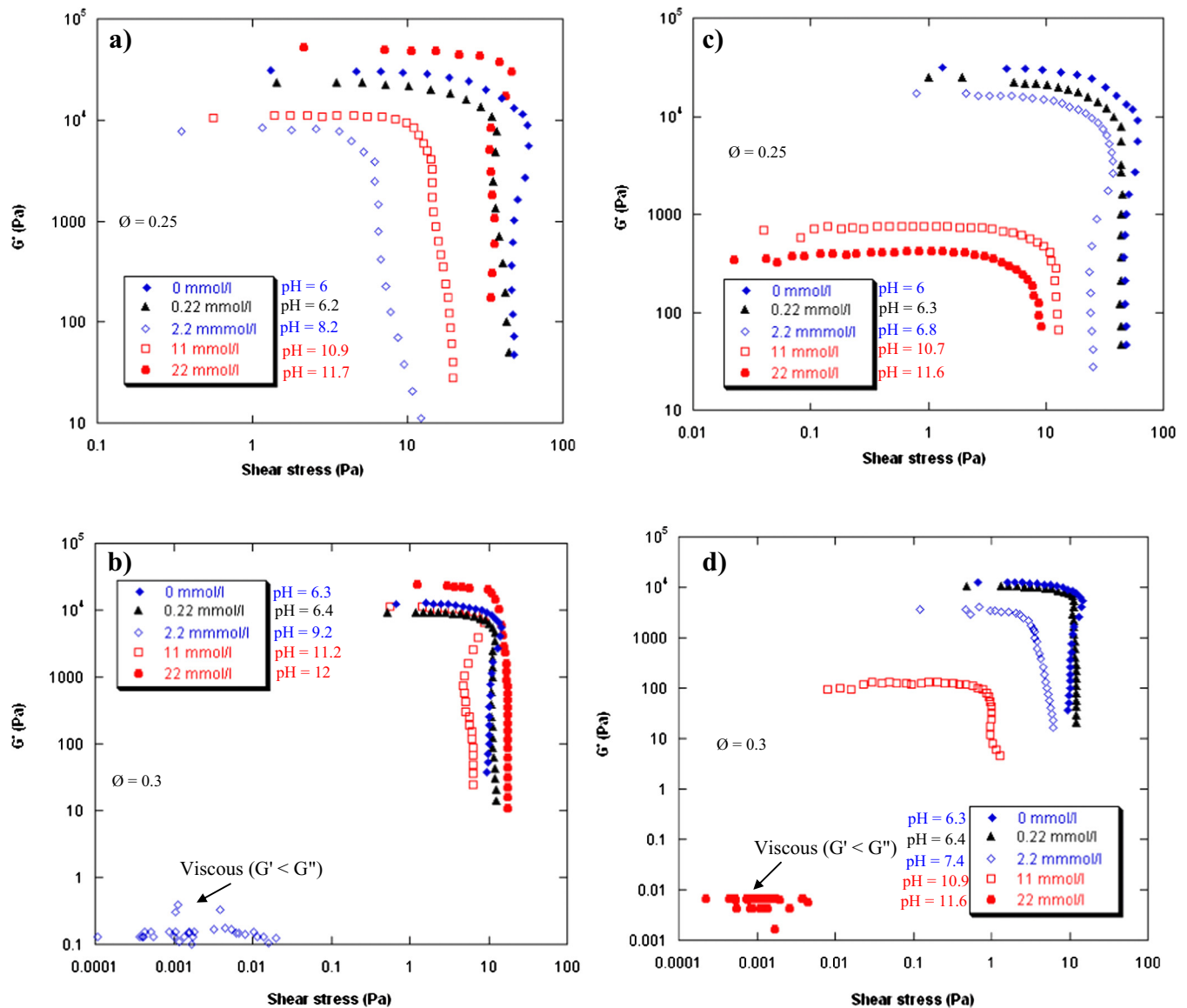
3.2. Rheological properties

3.2.1. Viscoelastic behaviors

3.2.1.1. Response to oscillatory shearing

3.2.1.1.1. Linear viscoelastic domain. At low strain amplitude ($\gamma < \gamma_{cr}$) both G′ and G″ exhibit a constant value regardless of strain amplitude (Fig. 2 & 4) suggesting that the relative displacement of the Kaol particles is negligible or weak to disrupt the gel structure. In other words, the network structure between Kaol particles is strong enough to resist the motion induced by oscillatory shearing. Thus, similar to τ_B, the parameters obtained prior to the structure breakdown (i.e. $G_0′$, γ_{cr} and cohesive energy density (E_c)) can be used as measure of inter-particle interactions.

The maximum stress that the dispersion withstands before acquiring a non-linear viscoelastic behavior (γ_{cr}) decreased first at lower concentration of Ca(OH)$_2$ (≤ 5.5 mmol/l), increasing at higher concentration (≥ 11 mmol/l) (Fig. 4a & b). The elastic component of the complex modulus in the viscoelastic region ($G′_0$) also followed the same trend (Fig. 5), suggesting that the gel structure of the Kaol

Fig. 4. Storage modulus (G′) vs. shear stress (at frequency of 1 Hz) of Kaol dispersions a) KGa-2 and b) KGa-1b as a function of Ca(OH)$_2$ concentration and c) KGa-2 and d) KGa-1b as a function of NaOH concentration.
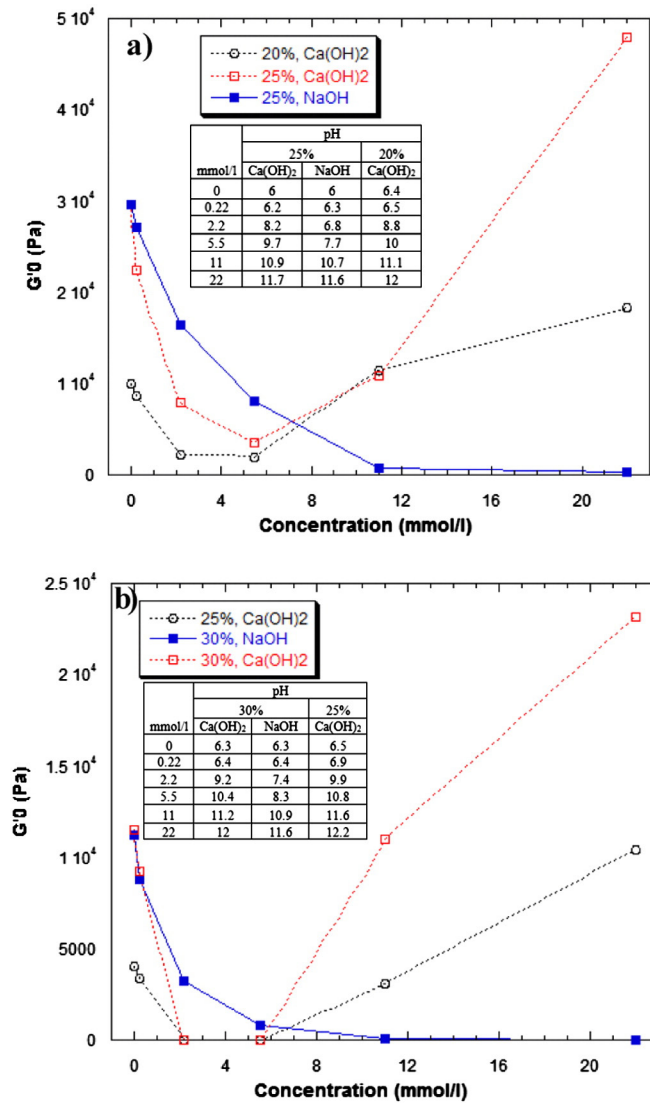
	pH		
	25%		20%
mmol/l	Ca(OH)₂	NaOH	Ca(OH)₂
0	6	6	6.4
0.22	6.2	6.3	6.5
2.2	8.2	6.8	8.8
5.5	9.7	7.7	10
11	10.9	10.7	11.1
22	11.7	11.6	12

	pH		
	30%		25%
mmol/l	Ca(OH)₂	NaOH	Ca(OH)₂
0	6.3	6.3	6.5
0.22	6.4	6.4	6.9
2.2	9.2	7.4	9.9
5.5	10.4	8.3	10.8
11	11.2	10.9	11.6
22	12	11.6	12.2

Fig. 5. Storage modulus in the linear viscoelastic region (G'_0) of Kaol dispersions a) KGa-2 and b) KGa-1b as a function of Ca(OH)₂ and NaOH concentrations.

dispersion can be broken more easily at lower concentration of Ca(OH)₂ due to dominant repulsive electrostatic interaction. On the other hand, further addition of Ca(OH)₂ (≥ 11 mmol/l), induced attractive inter-particle interaction. Hence, the structure became stiffer. The G'' changed in a similar way (data not shown) but the absolute values were smaller by more than one order of magnitude except for the KGa-1b slurry with 2.2 and 5.5 mmol/l Ca(OH)₂ which exhibited viscous behavior ($G'' > G'$). In the case of dispersions with NaOH, both parameters (G' and γ_{cr}) decreased monotonously with increasing NaOH concentration (Fig. 4c, d, 5) suggesting that the behavior at higher pH depends on the nature of the cation. Calcium undergoes hydrolysis at pH >10 forming CaOH⁺ (Mpofu et al., 2003, 2005). As a consequence, the apparent increase in gel strength at higher Ca(OH)₂ concentration is most likely caused by specific adsorption of CaOH⁺ that may favor linkage between Kaol particles. The same behavior was observed from the flow curve measurement analysis as described in Section 3.2.2.

The Ec, which corresponds to the work needed to break the gel structure (Tadros, 1996; Duran et al., 2000; Bossard et al., 2007), was calculated with the mean value of G' in the linear viscoelastic region using Eq. (5) and the data was plotted in Fig. 12 (Section 3.2.3) as a function of Ca(OH)₂ and NaOH concentrations. Ec depends on the

concentration of Ca(OH)₂ in a fashion completely similar to that corresponding to τ_B confirming that the gel-like structure of Kaol particles is weaker at lower and stiffer at higher concentration of Ca(OH)₂. In the case of NaOH, an increase in negative surface charge and electrostatic repulsion between Kaol particles reduced Ec with increasing NaOH concentration.

$$Ec = 1/2\gamma_{cr}^2 G'\tilde{A}_0 \quad (3)$$

3.2.1.1.2. Non-linear viscoelastic domain. At higher strain amplitude ($\gamma > \gamma_{cr}$), G' decreased gradually with increasing shear strain amplitude suggesting breakdown of the inter-particle network while G'' exhibited strain hardening characterized by hump with maximum value (G''_{max}) for strain amplitude γ_{max} (Fig. 2) due to restriction of shear-induced fluctuation of inter-particle distance (particle motion) by long range electrostatic repulsion and excluded volume interaction (Bossard et al., 2007) between neighboring plate-like Kaol particles. This strain hardening behavior of dispersions depends both on inter-particle distance and repulsive electrostatic forces (Bossard et al., 2007). In
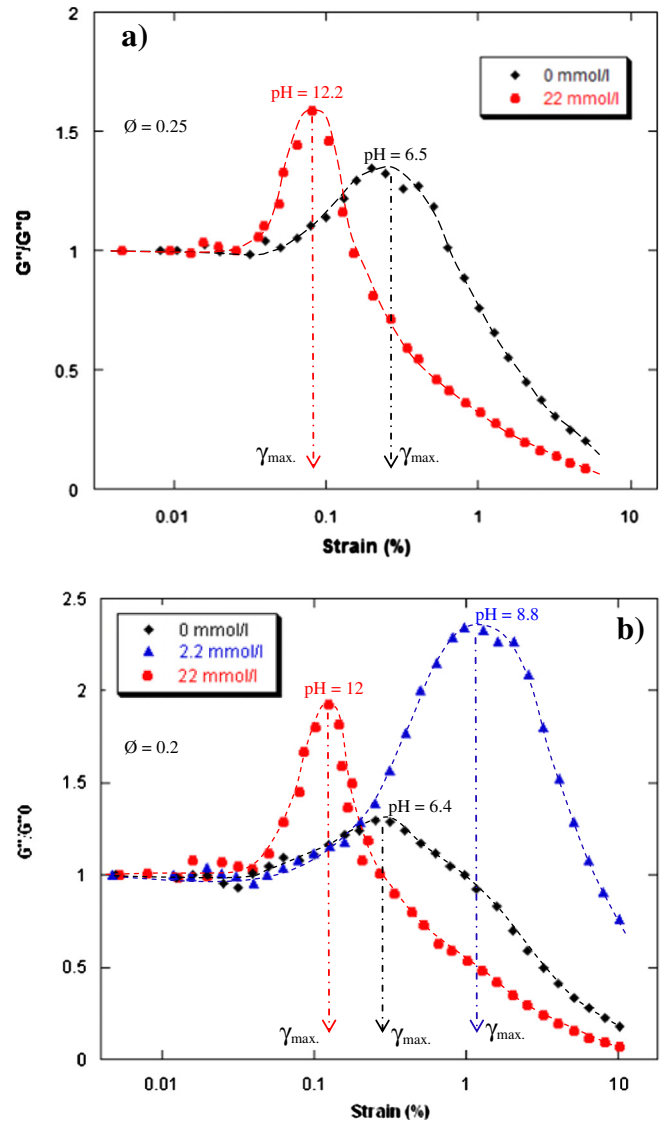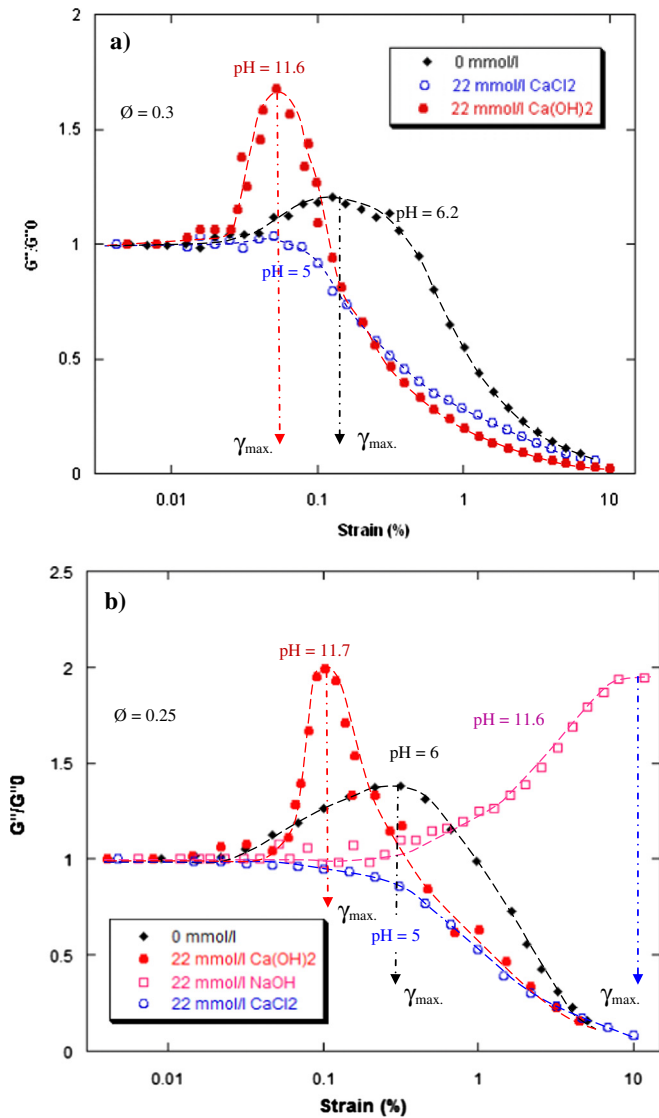

Fig. 6. Reduced loss modulus (G''/G''_0) as a function of strain amplitude of Kaol dispersion, a) KGa-1b and b) KGa-2 for different concentration of Ca(OH)₂. KGa-1b dispersion in the presence of 2.2 mmol/l Ca(OH)₂ exhibited viscous behavior.
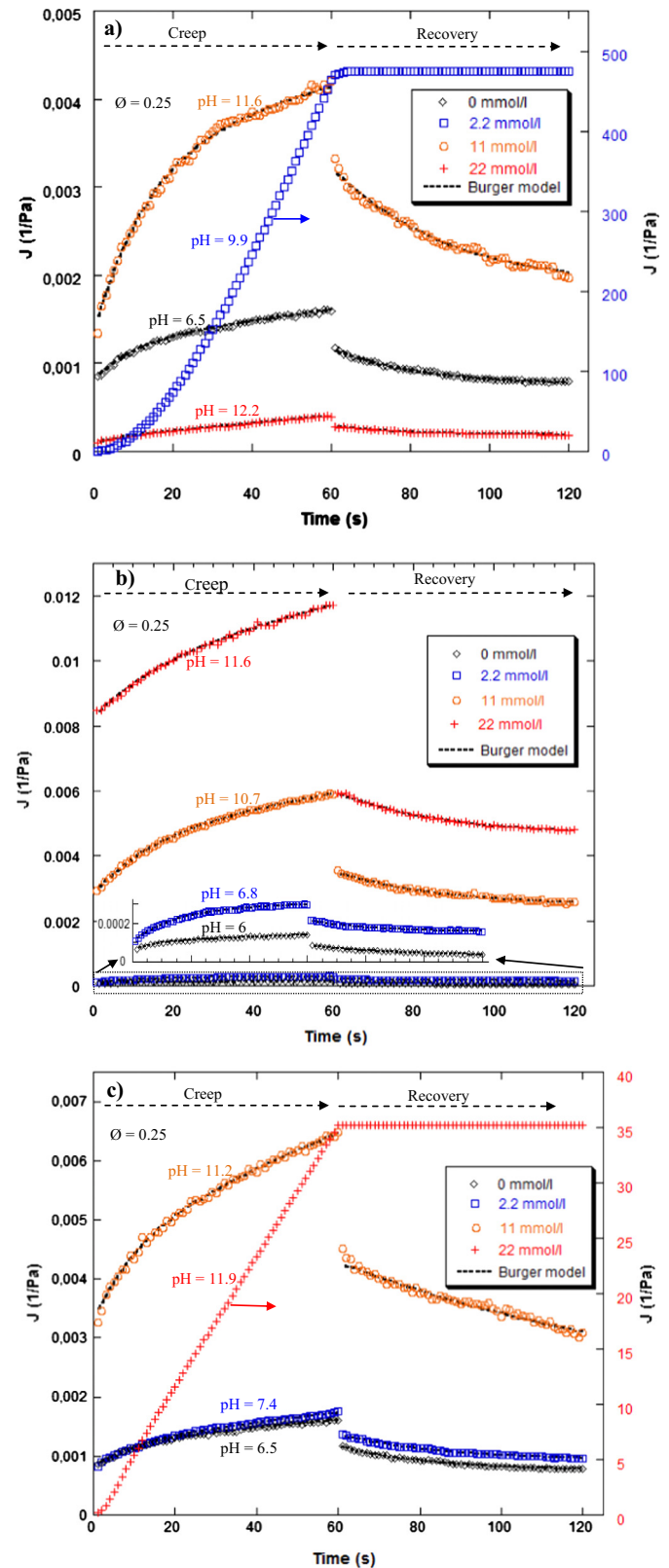
Fig. 7. Reduced loss modulus (G″/G″$_0$) as a function of strain amplitude of Kaol dispersion, a) KGa-1b and b) KGa-2 for different pH (Ca(OH)$_2$ vs. CaCl$_2$) and cation (Ca(OH)$_2$ vs. NaOH). KGa-1b dispersion with 22 mmol/l NaOH exhibited viscous behavior.

that the microstructural organization of the Kaol particles in the two conditions is different.

Under the pH condition of Kaol dispersion in de-ionized water (pH <6.2), the electrostatic attraction between positively charged

Fig. 8. Creep–recovery compliance (J) curve of Kaol dispersions a) KGa-2 and b) KGa-1b as a function of Ca(OH)$_2$ concentration and c) KGa-2 and d) KGa-1b as a function of NaOH concentration. The solid line represents the fitting to Burger model.

this work therefore, the nature of the G″ curve (i.e. relative change regardless of its physical meaning) of Kaol dispersion in the presence of different Ca(OH)$_2$ concentration were considered (Fig. 6 & 7), which may provide further knowledge about the microstructural organization of Kaol particles, such as the density of gel structure (closely packed or porous structure).

Let us first compare the dispersion in saturated lime solution (22 mmol/l Ca(OH)$_2$) and pure de-ionized water. Although the Kaol dispersions in both cases formed an attractive gel structure, characterized by higher τ_B and Ec, the response to oscillatory shearing in non-linear viscoelastic region is different in terms of width of strain hump, intensity of strain hardening and strain max (strain at G″$_{max}$). Strain hardening is more intense in the presence of 22 mmol/l Ca(OH)$_2$ than in pure de-ionized water. It means that, the interaction between adjacent Kaol particles, which depends on the inter-particle distance and surface charge (Bossard et al., 2007), is more intense in the former case. In addition, the relative width of the strain hump is lower (narrower) in the presence of 22 mmol/l Ca(OH)$_2$ than in de-ionized water, signifying that the motion of Kaol particles (inter-particle distance fluctuation) induced by oscillatory shearing is more restricted in the former case. From these observations, it is evident

edge and negatively charged tetrahedral faces yields E–F structure (Tombacz and Szekeres, 2006) characterized by high void ratios or porosity (Nasser and James, 2006; Du et al., 2010). This means that in E–F structures there is larger space for motion of Kaol particles. Hence more inter-particle distance fluctuation is expected once the gel structure or the linkages between particles are disturbed and particles are forced to move. This can explain the observed wider strain range over which strain hardening occurred (wider strain hump) for dispersions in de-ionized water compared to saturated lime solutions. Besides, the face–face inter-particle distance is relatively higher in E–F structures, which minimizes the strong electrostatic repulsion or excluded volume interaction between the larger basal faces of Kaol particles. The repulsion between an edge and a basal face is smaller than between two basal faces even if the charge densities are the same. As a result, the intensity of hardening is lower compared to Kaol dispersion in saturated lime solution where basal face–basal face interaction is expected to dominate (see below).

On the other hand, under the pH condition of saturated lime solution (pH >11), although all the surface of Kaol particles is expected to be negatively charged (Huertas et al., 1998; Tombacz and Szekeres, 2006), the adsorption of calcium ions counteracts the effect of pH in increasing negative surface charge (Fig. 3). This is attributed to the formation and adsorption of the first hydrolysis product of Ca-ions ($CaOH^+$) on the deprotonated octahedral faces and edge sites of Kaol as it is confirmed in the present work (Section 3.1.2). In saturated lime solution, thus, it is expected that the higher negative potential on alumina and edge faces of Kaol particles would strongly attract and bind $CaOH^+$ close to the surface of octahedral and lateral faces, and subsequently, would form an electropositive site. The presence of electropositive sites on the surface of Kaol at higher pH (pH >10) and in the presence of hydrolysable metal ions such as Ca(II) and Mn(II) has been reported previously (Shankar et al., 2010; Avadiar et al., 2012, 2014). In these studies the adsorption of anionically charged polyacrylamids (PAM) on Kaol surface at pH = 10.5 was significantly improved by prior addition of Ca(II) ions implying a positively charged Kaol surface. Therefore, the adsorption of $CaOH^+$ can allow attraction with negatively charged silica faces (Avadiar et al., 2012, 2014). This interaction forms alumina face–silica face and edge face–alumina face aggregated microstructures. However, because of plate like particles and limited edge area compared to the basal planes, F–F interaction is more probable at the beginning of aggregation, yielding dense, tightly packed flake-like structures (Nasser and James, 2006; Du et al., 2010). In these closely packed structures, the interactions between neighboring particles are intense because of closer particle distance and large area of F–F interaction, hence increasing the intensity of strain hardening. The oscillatory shear induced fluctuation of inter-particle distances are also restricted due to the closely packed structure. This can explain the observed relatively narrow strain hump. Furthermore, the contribution of edges will also become similar to that of faces (higher surface area over which interaction occurs) as the thickness and edge area

increase when the Kaol particles are stacked due to the silica face–alumina face interaction.

In the presence of lower concentration of Ca(OH)₂ (≤5.5 mmol/l) and with increasing the concentration of NaOH, the influence of pH on increasing surface charge dominates over the neutralization of the

Table 4
Fitting parameters of the creep–recovery data in Fig. 8 & 9 (KGa-1b).

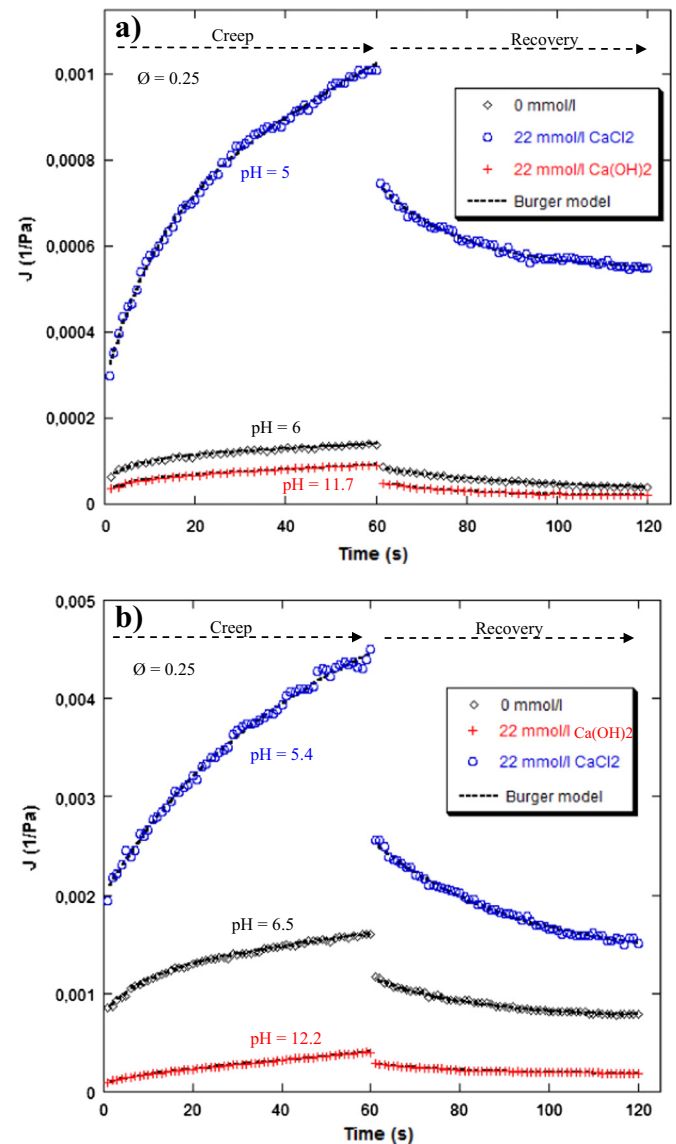|	mmol/l	pH	Creep				Recovery		
			J_0 (10^{-5} 1/Pa)	J_1 (10^{-5} 1/Pa)	t_1 (s)	η_0 (10^5 Pa/s)	J_0 (10^{-5} 1/Pa)	J_1 (10^{-5} 1/Pa)	t_1 (s)
Ca(OH)₂	0	6	5.9	4.58	7.6	17.1	8.7	5.3	16.7
	2.2	8.2	67.6	48.1	10.4	1.78	124.7	42.3	19.2
	11	10.9	12.6	16.2	9.8	4.19	30.6	8.47	19.6
	22	11.7	2.9	2.9	6.7	18	5.04	3.1	12.5
CaCl₂	22	5	28	40.1	11.9	1.73	75	20.6	18.7
NaOH	2.2	6.8	10.3	16.7	13.9	16.8	21.7	6.1	21.8
	11	10.7	279.9	189.1	15.3	0.48	354.3	107.8	25.8
	22	11.6	824	190	18.4	0.35	599.4	135.9	26.1

Table 5
Fitting parameters of the creep–recovery data in Fig. 8 & 9 (KGa-2).

	mmol/l	pH	Creep				Recovery		
			J_0 (10^{-5} 1/Pa)	J_1 (10^{-5} 1/Pa)	t_1 (s)	η_0 (10^5 Pa/s)	J_0 (10^{-5} 1/Pa)	J_1 (10^{-5} 1/Pa)	t_1 (s)
Ca(OH)₂	0	6.5	79.8	43.7	10	1.6	117	41.4	21.9
	2.2	9.9	–	–	–	–	–	–	–
	11	11.6	134.3	271	14.2	0.92	324	138.8	29.1
	22	12.2	8.7	6.2	7.4	2.4	28.9	10.3	18.4
CaCl₂	22	5.4	198.8	175.7	27.5	0.66	256.9	124.1	31.5
NaOH	2.2	7.4	80.3	45	10.6	1.2	136.8	44.3	25.7
	11	11.2	329.8	145.2	11.8	0.35	428	259.3	98.7
	22	11.9	–	–	–	–	–	–	–

Fig. 9. The effect of pH and calcium concentration on viscoelastic behavior of Kaol dispersions a) KGa-2 and b) KGa-1b.

charge by Ca and Na ions as it is indicated by the increase of negative zeta potential (Fig. 3). In this condition the Kaol particles are uniformly charged and are repelled from each other, forming a very porous gel structure. Consequently, the fluctuation of inter-particle distance induced by oscillatory shearing will be higher, thus explaining the observed high range of strain, over which strain hardening occurred (i.e. relatively wider strain hump). On the other hand, the higher intensity of strain hardening is attributed to strongly repulsive electrostatic interaction between the uniformly charged Kaol particles.

To verify the effect of pH, experiments were carried out, using $CaCl_2$ solution with similar Ca-ion concentration as the saturated lime solution ($[Ca^{2+}] = 22$ mmol/l), but different pH (pH = 5). The strain sweep curves of the Kaol dispersion in the two solutions are compared (Fig. 7). The behavior at higher amplitude is different in the two cases. In comparison to the slurries in de-ionized water, the intensity of strain hardening increased in the presence of 22 mmol/l $Ca(OH)_2$ while the dispersion in chloride solution (22 mmol/l $CaCl_2$) showed strain thinning behavior (i.e. both G′ and G″ decreased at $\gamma_0 > \gamma_{cr}$). As it was mentioned before, at pH lower than PZC of edge (pH ≈ 7), electrostatic attraction between oppositely charged edges and faces leads to E–F flocculated structure. However, it seems that the presence

of Ca ion weakens this interaction, probably due to screening of the surface charges at the silica face, followed by collapse of some of the E–F structure. This observation implies that the closely packed gel structure in saturated lime solution, characterized by higher strain hardening intensity and narrow strain hump, is caused by simultaneous occurrence of Ca- and OH-ions (higher pH).

3.2.1.2. Creep–recovery behavior. The evolution of deformation per unit stress (J) with time after application of shear stress (in the linear viscoelastic region ≤1 Pa) for different hydrated lime concentrations is indicated in Fig. 8. At t = 60 s, the stress is removed, and the deformation is followed (recovery process). It is clear that the deformation increased first at lower concentration of $Ca(OH)_2$ (2.2 mmol/l) and decreased for higher concentration of $Ca(OH)_2$ (22 mmol/l). This is a characteristic of a system with weak and strong links in their internal gel structures, respectively. With systems containing NaOH, the creep deformation increased monotonously with increasing NaOH concentration, indicating a shift from flocculated to deflocculated gel structure or sol (no recovery in the case of KGa-1b with 22 mmol/l NaOH) due to an increase in repulsive electrostatic force between particles.
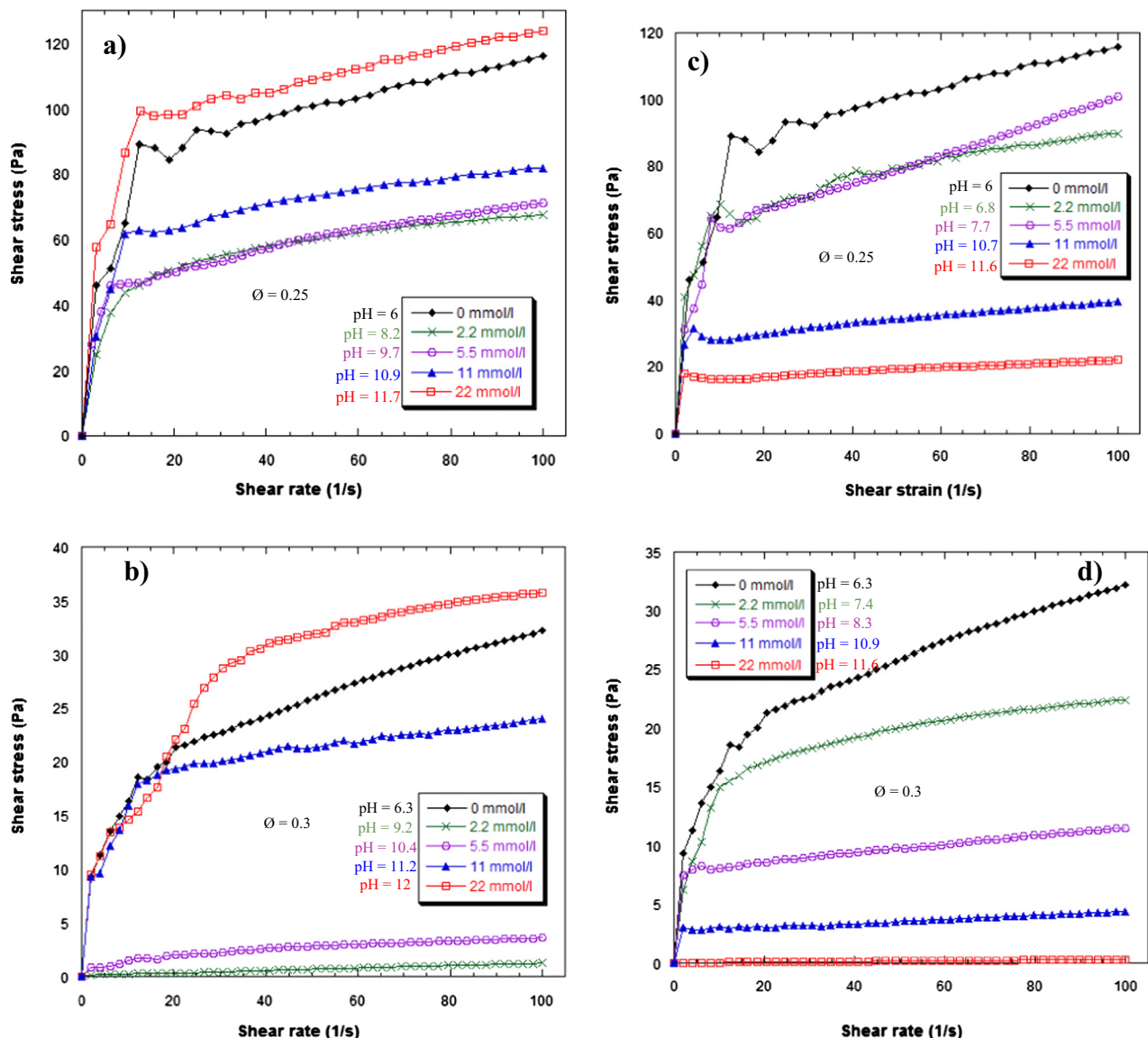

Fig. 10. Flow curve of Kaol dispersions a) KGa-2 and b) KGa-1b as a function of $Ca(OH)_2$ concentration and c) KGa-2 and d) KGa-1b as a function of NaOH concentration.

The continuous lines drawn in Fig. 8 are the results of fitting the creep–recovery data to Burger model, a combination of Maxwell (represented by spring and dashpot) and Kelvin–Voigt elements (parallel arrangement between spring and dashpot) (Tadros, 1996; Nasser and James, 2006). The creep curves are described by four elements model as follows (Eq. (4)):

$$J_c(t) = J_0 + J_1(1 - \exp(-t/t_1)) + t/\eta_0. \tag{4}$$

The recovery curves are represented without the pure viscous (dashpot) parameter as the slurry goes to equilibrium up on release of stress as follows (Eq. (5)):

$$J_r(t) = J_0 + J_1(\exp(-t/t_1) - 1). \tag{5}$$

In Eqs. 4 and 5, J_0, J_1, η_0 and t_1 are instantaneous elastic compliance, the retarded elastic compliance, viscosity and relaxation time, respectively. The fitting parameters are summarized in Tables 4 & 5. The J_0 and J_1 both for creep and recovery curve showed first an increasing trend (less stiff) at lower concentration of $Ca(OH)_2$ (2.2 mmol/l) and then decreased (became stiffer) for higher concentration of $Ca(OH)_2$ (11 & 22 mmol/l). The parameter η_0, associated to the viscosity in the Newtonian regime (dashpot), decreased in lower (2.2 mmol/l) and increased in higher (11 & 22 mmol/l) concentration of $Ca(OH)_2$. In contrary to these observations, J_0 and J_1 increased and η_0 decreased continuously with increasing NaOH concentration, indicating progressive weakening of linkages between Kaol particles. The t_1, which is related to the recovery properties of the system (Duran et al., 2000), increased at lower concentration of $Ca(OH)_2$ and with increasing the concentration of NaOH in Kaol slurries revealing that the restoring force is low and the system needs longer time to reach equilibrium. It means that Na-ions and low concentration of Ca ($\leq$2.2 mmol/l $Ca(OH)_2$) cannot overcome the repulsion force between uniformly charge Kaol particles and network cannot be formed. On the other hand, t_1 decreased for Kaol slurries with higher $Ca(OH)_2$ concentration (11 & 22 mmol/l), suggesting that Ca-ion in such conditions induces linkage between Kaol particles and improves the recovery properties of Kaol dispersion.

In Fig. 9 the creep–recovery behavior of Kaol slurries in de-ionized water (0 mmol/l, pH = 6), lime solution (22 mmol/l $Ca(OH)_2$, pH = 11.9) and chloride solution (22 mmol/l $CaCl_2$, pH $\approx$ 5) was compared. The parameters J_0, J_1 and t_1 increased and η_0 decreased in the case of $CaCl_2$ solution (Tables 4 & 5), suggesting a weak gel structure, compared to the saturated lime solution and de-ionized water. At pH <7, the gel structure is due to E–F (tetrahedral face) association of Kaol particles (Van Olphen, 1964; Tombacz and Szekeres, 2004, 2006). However, the presence of cations, such as Ca^{2+}, shields the permanent charge on tetrahedral face, leading to partial E–F breakdown of the structure, which can explain the weak gel structure (reflected by higher J_0, J_1 and t_1) in the case of $CaCl_2$ solution. However, in Ca-rich alkaline conditions (saturated lime solution), it seems that the Ca-ions have prominent influence in linking the Kaol particles, thereby inhibiting free movement and increasing the viscosity, resulting in the sharply decrease of the permanent deformation, which is reflected by lower compliance (J_0 and J_1) and higher η_0. Therefore, an increase in the rigidity of Kaol dispersions after lime treatment could not only be explained by higher concentration of Ca ion, but by simultaneous occurrence of Ca and OH ions (higher pH) in accordance with the results of dynamic (oscillatory) measurements (Section 3.2.1.1).

3.2.2. Bingham yield stress

In both samples, the flow curve shifted first to lower and then to higher shear stress with adding lower ($\leq$5.5 mmol/l) and higher (>11 mmol/l) concentration of $Ca(OH)_2$, respectively, whereas it shifted gradually to lower values with increasing concentration of NaOH (Fig. 10). The τ_B was used as a measure of particle interactions in the dispersion in the presence of different concentrations of $Ca(OH)_2$ and NaOH. Two stage changes in τ_B were observed (Fig. 11): first decreased with increasing concentration up to 5.5 mmol/l, increasing concentration at $\geq$11 mmol/l. In aqueous solutions, $Ca(OH)_2$ dissociates into Ca^{2+} and OH^- ions. These ions have opposite effect on the interaction of clay mineral particles (i.e. OH-ions increase the negative surface charge resulting in repulsion, whereas Ca-ions counteract this effect by neutralizing the negative surface charge). The overall interaction is, therefore, determined by the combined effect of the two ions.

In lime free solution, the pH of the dispersion (pH $\approx$ 6) is lower than the PZC of edge (pH$_{PZC, edge} \approx$ 7) (Tombacz and Szekeres, 2006). Hence the edges are expected to be positively charged and the tetrahedral face has constant negative charge causing greater force of attraction between the Kaol particles in E–F flocculation, and yielding strong flocs. Consequently, the stress required to fully disrupt the flocs, τ_B, is higher as well. As the pH increases, the negative surface charge increases due to deprotonation of functional groups and the inter-particle force becomes repulsive. At lower $Ca(OH)_2$ concentration ($\leq$5.5 mmol/l), the effect of pH appeared to dominate over the effect of Ca-ion to neutralize the surface charge, thereby increasing the repulsion between particles with increasing concentration. The net effect is then to weaken the floc strength which is reflected by the decrease in the τ_B. On the other
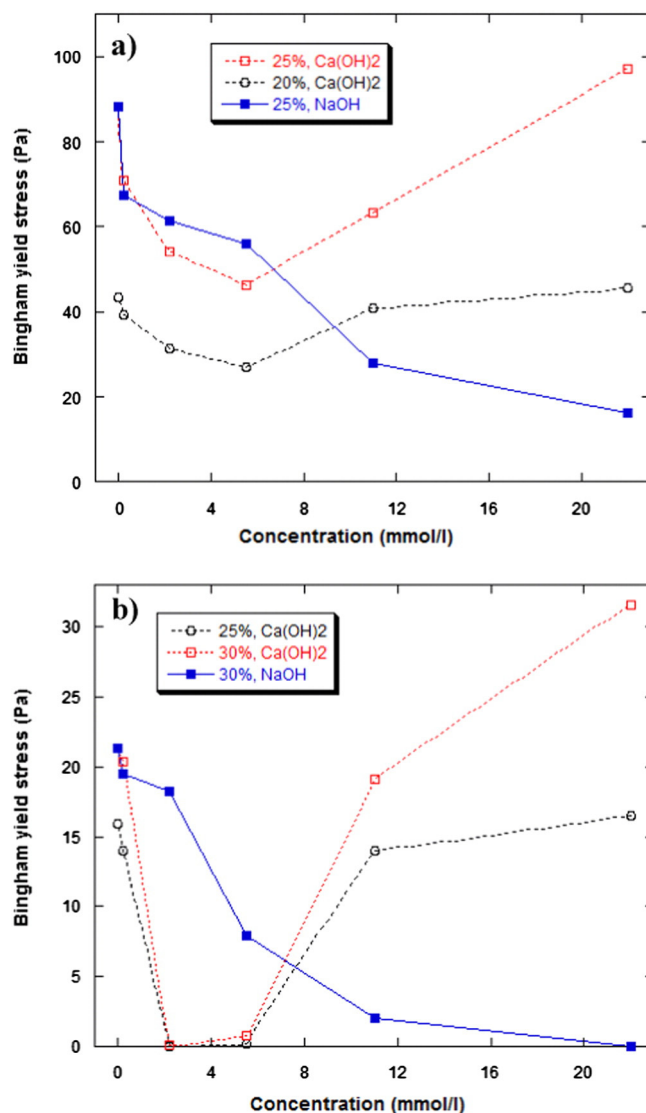

Fig. 11. Bingham yield stress of Kaol dispersion, 20–30 mass% solid, a) KGa-2 and b) KGa-1b in the presence of $Ca(OH)_2$ and NaOH. Please refer to Fig. 5 for the pH of the dispersions.
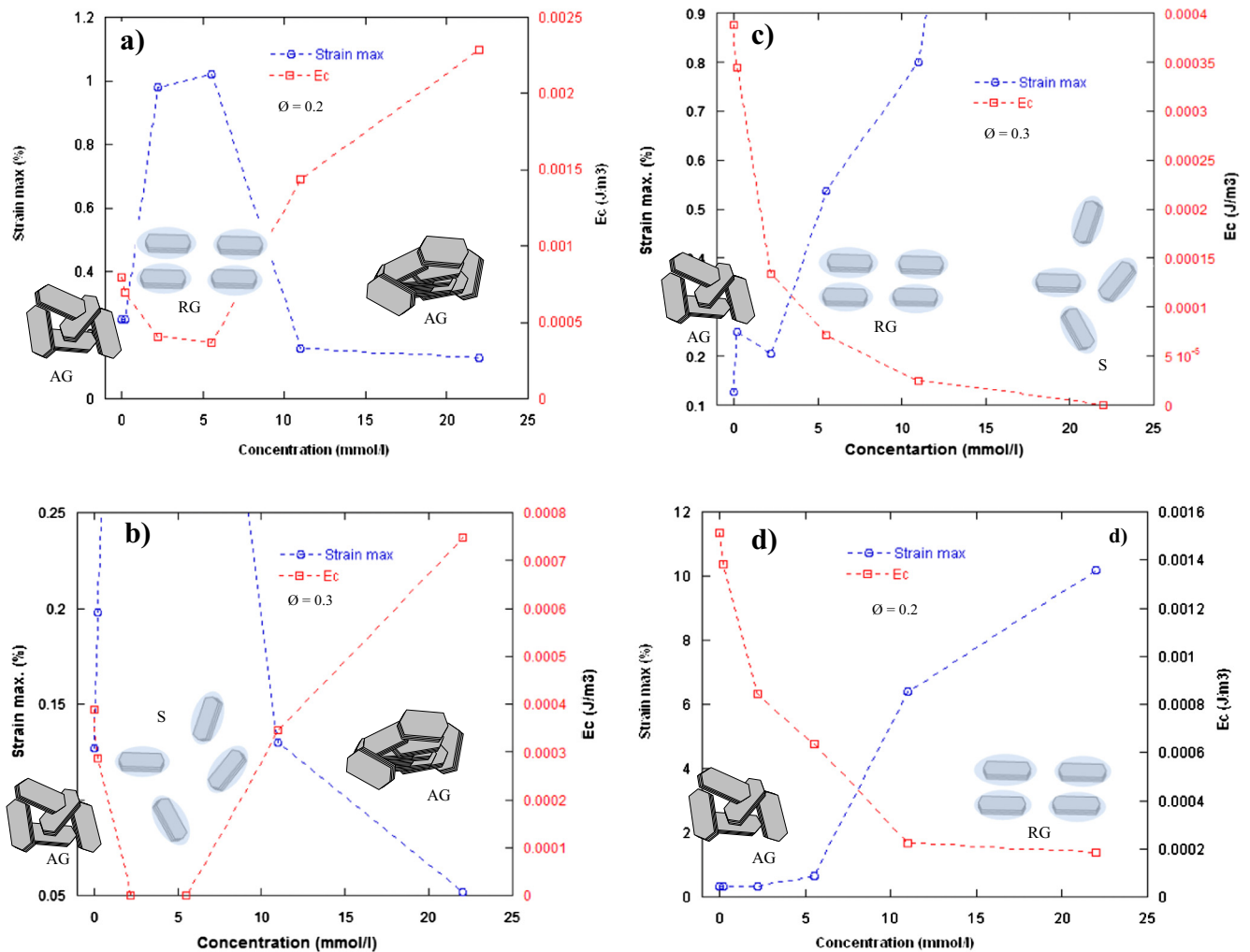
hand, at higher concentration (≥ 11 mmol/l) and pH (pH >10), where both octahedral and edge faces are expected to be negative (Huertas et al., 1998; Tombacz and Szekeres, 2006), the increase in Ca(OH)$_2$ concentration reduced the magnitude of zeta potential (Fig. 3) and increased τ_B. High yield stress at higher pH with high Ca(II) content was also observed by Avadiar et al. (2012, 2014) and Au and Leong (2013) for Unimin Kaol. These workers considered that it is possible to have a net attractive force between positive charged (edge and octahedral face) and negatively charged (tetrahedral) surfaces at higher pH, due to adsorption of hydrolysed species of Ca(II) (CaOH$^+$). In addition, Shankar et al. (2010) observed total elimination of the high yield stress by adsorption of negatively charged phosphate additive, further supporting the hypothesis of opposite charge attraction between Kaol particles. This opposite charge particle interaction leads to flocculation which is reflected by the increase in τ_B. In the case of dispersions containing NaOH, the τ_B decreased monotonously with increasing the concentration of NaOH, supporting the suggestion that the behavior at higher pH depends on the nature of the cation (i.e. hydrolysable vs. non-hydrolysable).

The difference in the rheological properties observed between the two samples can be probably be assigned to the difference in crystal order and associated morphology. Indeed, higher τ_B was observed for high defect Kaol (KGa-2) than low defect Kaol (KGa-1b) at the same particle concentration. The pseudo-hexagonal flakes in KGa-1b Kaol appeared to be thicker (large number of layer stacking) than KGa-2

Kaol (Fig. 1). The larger the number of layer stacking and thicker the particle, the lower the number of particle interactions and the weaker the linkages between those interactions and vice versa as it has been observed for the case of smectite (Abend and Lagaly, 2000; Christidis et al., 2006; Laird, 2006; Chemeda et al., 2014). In other words, the physico-chemical inter-particle forces are relatively smaller in low defect Kaol because of low specific surface area. This could explain the observed lower yield stress of KGa-1b than KGa-2 dispersions.

3.2.3. Sol, repulsive gel and attractive gel

The Ec and γ_{max} determined from the oscillatory experiment were plotted as a function of concentrations of NaOH and Ca(OH)$_2$ (Fig. 12) and were used with the creep–recovery experimental results to distinguish the different state of Kaol dispersion. Evidently, distinction was made between attractive gel, repulsive gel and sol. First, the creep–recovery experimental result was used to distinguish sol and gel. The sol did not show recovery upon release of stress (e.g. KGa-1b slurry with 2.2 and 5.5 mmol/l Ca(OH)$_2$ and 22 mmol/l NaOH), whereas the gel showed partial recovery (Fig. 8). Since no viscoelastic behavior is observed in the sol (i.e. G' < G'', viscous dispersions) under dynamic conditions, the values of Ec and γ_{max} are considered to be zero (no particle linkage) and infinite (excessive deformation), respectively. In sol (stable viscous dispersion), the Kaol particles are free to move and can easily shift with respect to each other exhibiting excessive deformation upon shearing. The repulsive gel, which formed at lower concentration

Fig. 12. Strain max. (γ_{max}) and cohesive energy density (Ec (J/m^3)), as a function of concentration of Ca(OH)$_2$, a) KGa-2 & b) KGa-1b, and NaOH, c) KGa-1b & d) KGa-2, together with a schematic representation of the mode of particle association in the different state (i.e. attractive gel (AG), repulsive gel (RG) and sol (S)). For the sol (viscous slurry), γ_{max} and Ec considered to being infinite (excessive deformation) and zero, respectively, for the sake of comparison. Please refer to Fig. 5 for the pH of the dispersions.

of Ca(OH)$_2$ (e.g. KGa-2 slurry with 2.2 and 5.5 mmol/l) and with increasing concentration of NaOH, is characterized by lower and higher value of Ec and γ_{max}, respectively. The structure in the case of repulsive gel is attributed to strong inter-particle repulsive force that to a certain degree caused parallel orientation (Abend and Lagaly, 2000) of Kaol particles and restricted their free translational and rotational motion under shearing. On the other hand, the attractive gel, which evidently formed in de-ionized water at pH < pH$_{PZC, edge} \approx 7$, due to attractive force between oppositely charged edge and face and at higher concentration of Ca(OH)$_2$ due to linkage induced by Ca-ions, is characterized by relatively higher Ec and lower γ_{max} value.

3.3. Aggregate size

The average aggregate size of Kaol remains unchanged as a function of time both in de-ionized and NaOH solution (22 mmol/l), which represents a more dispersed state for the Kaol particles (Fig. 13). However, the average aggregate size in de-ionized water is slightly larger, which could be indicative of a smaller flocs formed mainly by edge–face associations. In contrast, the initial aggregate size of Kaol in saturated lime solution (22 mmol/l Ca(OH)$_2$) was at least four times higher than in de-ionized water and NaOH solution. Furthermore, the size of aggregate increased with time, which represents a strong flocculated structure. Note that also the rate of increase of aggregate size is lower initially and increased at longer contact time. This probably suggests that the Kaol particles in saturated lime solution are associated with different mode of interaction. As mentioned before, the electropositive sites that emerge as a consequence of adsorption of CaOH$^+$ leads to F–F (alumina face–silica face) and E–F (edge face–alumina face) aggregates (Avadiar et al., 2012). However, due to strong anisotropy of the Kaol particles, the contribution of edges is lower or insignificant, thus Kaol particles associate in F–F (alumina face–silica face) interaction mode at the beginning of aggregation. Subsequently, the thickness increases and the edge effect would become significant, and thereby the aggregate size increased more via both F–F and E–F particle associations. This increase in grain size is expected to reduce the reactivity with water. Therefore, the decrease in swelling and shrinkage potential of clayey soil after lime treatment is most likely related to flocculation of clay mineral particles in the presence of Ca and OH-ions.

4. Summary and conclusion

The present study assessed the effect of hydrated lime on surface property and Kaol particles interaction. Analysis of interfacial chemistry suggested that Kaol predominantly adsorbs Ca^{2+} and CaOH$^+$ at pH 7 and 12.6, respectively. The adsorption of the latter (CaOH$^+$) significantly influences the zeta potential and particle interaction. With increasing Ca(OH)$_2$ concentration, G', τ_B and Ec first decreased at lower concentration (≤ 5.5 mmol/l) and then increased at higher concentration (≥ 11 mmol/l). In the first stage, the repulsive electrostatic force is more significant and thus limited inter-particle collisions and aggregation of the particles, whereas in the second stage, Ca-ions counteracted electrostatic repulsion and induced linkage and aggregation of the particles. The simultaneous occurrence of hydrolysable cation such as Ca and higher pH is important for the behavior observed in the second stage, due to the modification of surface properties of Kaol particles by adsorption of the first hydrolysis species (CaOH$^+$). The non-linear viscoelastic behavior, in particular the intensity and relative width of strain hardening in G'' curve, is a good qualitative indicator of the density of gel structure. Compacted and open gel structures are characterized by relatively narrow and wider strain hump, respectively. On the other hand, the intensity of hardening is enhanced either with increasing long range electrostatic repulsion or with decreasing inter-particle distance between high area basal faces.

Overall, this study has shown that the short-term effect of lime treatment on mechanical properties of clayey soil is the consequence of
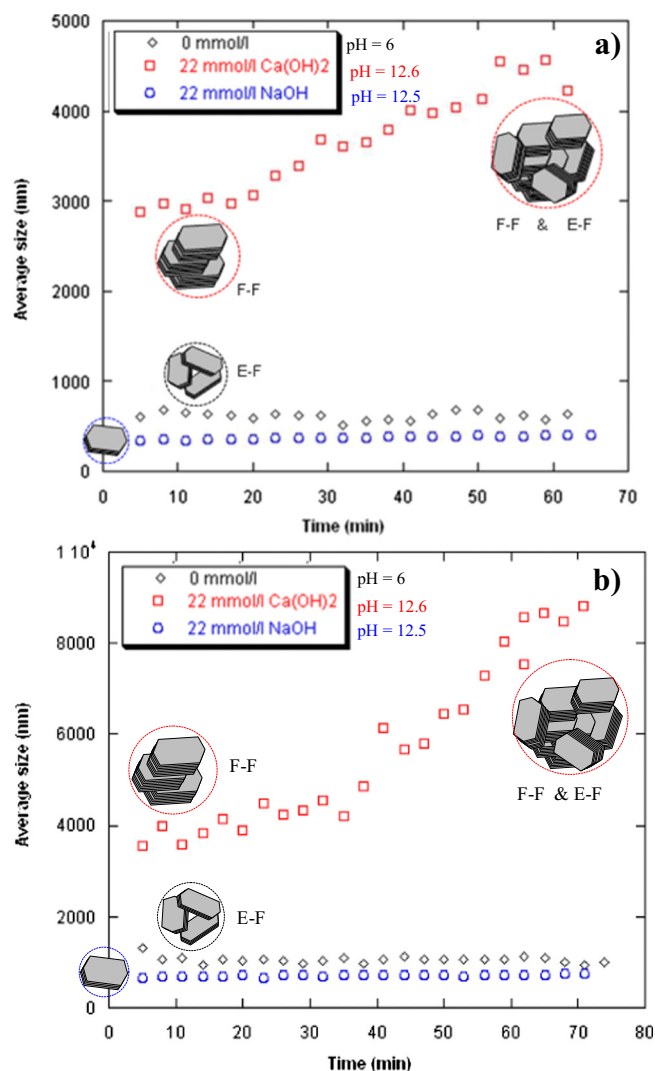

Fig. 13. Evolution of average floc size of Kaol dispersion, a) KGa-2 and b) KGa-1b, and a schematic representation of the mode of particle association.

calcium rich alkaline solution generated by lime addition and its effect on surface charge and the mode of particle association. Ca-ions at higher pH (CaOH$^+$) promote mainly F–F linkages between Kaol particles and are efficient in forming tightly packed flocs with lower deformation. The flocs behave as individual coarse grained material (silt or sand). Thus, their reactivity with water is expected to be reduced upon exposure to moisture, which in turn lowers the swelling and shrinkage potential and improves their workability.

References

Abend, S., Lagaly, G., 2000. Sol–gel transitions of sodium montmorillonite dispersions. Appl. Clay Sci. 16, 201–227.
Al-Mukhtar, M., Lasledj, A., Alcover, J.-F., 2010. Behaviour and mineralogy changes in lime-treated expansive soil at 20 °C. Appl. Clay Sci. 50, 191–198.
Atesok, G., Somasundaran, P., Morgan, L.J., 1988. Adsorption properties of Ca^{2+} on Na–kaolinite and its effect on flocculation using polyacrylamides. Colloids Surf. 32, 127–138.
Au, P.-I., Leong, Y.-K., 2013. Rheological and zeta potential behaviour of kaolin and bentonite composite slurries. Colloids Surf. A Physicochem. Eng. Asp. 436, 530–541.

Avadiar, L., Leong, Y., Fourie, A., Nugraha, T., 2012. Rheological response to Ca(II) concentration — the source of kaolin slurry rheological variation. Chemeca 2012 Conference,Wellington, New Zealand, 23–26 September.

Avadiar, L., Leong, Y., Fourie, A., Nugraha, T., Clode, P.L., 2014. Source of kaolin slurry rheological variation-Ca^{2+} concentration. Colloids Surf. A Physicochem. Eng. Asp. 459, 90–99.

Bell, F.G., 1996. Lime stabilisation of clay minerals and soils. Eng. Geol. 42, 223–237.

Bossard, F., Moan, M., Aubry, T., 2007. Linear and nonlinear viscoelastic behavior of very concentrated plate-like kaolin suspensions. J. Rheol. 51, 1253–1270.

Chemeda, Y.C., Christidis, G.E., Tauhid Khan, N.M., Koutsopoulou, E., Hatzistamou, V., Kelessidis, V.C., 2014. Rheological properties of palygorskite–bentonite and sepiolite–bentonite mixed clay suspensions. Appl. Clay Sci. 90, 165–174.

Choquette, M., Berube, M.-A., Locat, J., 1987. Mineralogical and microtextural changes associated with lime stabilization of marine clays from Eastern Canada. Appl. Clay Sci. 2, 215–232.

Christidis, G.E., Blum, A.E., Eberl, D.D., 2006. Influence of layer charge and charge distribution of smectites on the flow behaviour and swelling of bentonites. Appl. Clay Sci. 34, 125–138.

Diamond, S., Kinter, E.B., 1965. Mechanisms of soil–lime stabilization. Highw. Res. Rec. 92, 83–102.

Du, J., Morris, G., Pushkarova, R.A., Smart, R.S.C., 2010. Effect of surface structure of kaolinite on aggregation, settling rate, and bed density. Langmuir 26 (16), 13227–13235.

Duran, J.D.G., Ramos-Tejada, M.M., Arroyo, F.J., Gonzalez-Caballero, F., 2000. Rheological and electrokinetic properties of sodium montmorillonite suspensions: I. Rheological properties and interparticle energy of interaction. J. Colloid Interface Sci. 229, 107–117.

Eisazadeh, A., Kassim, K.A., Nur, H., 2012. Solid-state NMR and FTIR studies of lime stabilized montmorillonite and lateritic clays. Appl. Clay Sci. 67–68, 5–10.

Gupta, V., Hampton, M.A., Stokes, J.R., Nguyen, A.V., Miller, J.D., 2011. Particle interactions in kaolinite suspensions and corresponding aggregate structures. J. Colloid Interface Sci. 359, 95–103.

Huertas, J.F., Chou, L., Wollast, R., 1998. Mechanism of kaolinite dissolution at room temperature and pressure: part 1. Surface speciation. Geochim. Cosmochim. Acta 62, 417–431.

Hyun, K., Kim, S.H., Ahn, K.H., Lee, S.J., 2002. Large amplitude oscillatory shear as a way to classify the complex fluids. J. Non-Newtonian Fluid Mech. 107, 51–65.

James, R.O., Healy, T.W., 1972. Adsorption of hydrolyzable metal ions at the oxide–water interface I. Co(ll) adsorption on SiO$_2$ and TiO$_2$ as model systems. J. Colloid Interface Sci. 40, 42–52.

Johnson, S.B., Russell, A.S., Scales, P.J., 1998. Volume fraction effects in shear rheology and electroacoustic studies of concentrated alumina and kaolin suspensions. Colloids Surf. A Physicochem. Eng. Asp. 141, 119–130.

Kavak, A., Baykal, G., 2012. Long-term behaviour of lime-stabilized kaolinite clay. Environ. Earth Sci. 66, 1943–1955.

Konan, K.L., Peyratout, C., Smith, A., Bonnet, J.-P., Rossignol, S., Oyetola, S., 2009. Comparison of surface properties between kaolin and metakaolin in concentrated lime solutions. J. Colloid Interface Sci. 339, 103–109.

Kretzschmar, R., Holthoff, H., Sticher, H., 1998. Influence of pH and humic acid on coagulation kinetics of kaolinite: a dynamic light scattering study. J. Colloid Interface Sci. 202, 95–103.

Laird, D.A., 2006. Influence of layer charge on swelling of smectites. Appl. Clay Sci. 34, 74–87.

Locat, J., Berube, M.A., Choquette, M., 1990. Laboratory investigations on the lime stabilisation of sensitive clays: shear strength development. Can. Geotech. J. 27, 294–304.

Mpofu, P., Addai-Mensah, J., Ralston, J., 2003. Influence of hydrolyzable metal ions on the interfacial chemistry, particle interactions, and dewatering behavior of kaolinite dispersions. J. Colloid Interface Sci. 261, 349–359.

Mpofu, P., Addai-Mensah, J., Ralston, J., 2005. Interfacial chemistry, particle interactions and improved dewatering behaviour of smectite clay dispersions. Int. J. Miner. Process. 75, 155–171.

Nasser, M.S., James, A.E., 2006. Settling and sediment bed behaviour of kaolinite in aqueous media. Sep. Purif. Technol. 51, 10–17.

Nasser, M.S., James, A.E., 2008. Degree of flocculation and viscoelastic behaviour of kaolinite–sodium chloride dispersions. Colloids Surf. A Physicochem. Eng. Asp. 315, 165–175.

Olphen, H.V., 1964. Internal mutual flocculation in clay suspension. J. Colloid Sci. 19, 313–322.

Penner, D., Lagaly, G., 2001. Influence of anions on the rheological properties of clay mineral dispersions. Appl. Clay Sci. 19, 131–142.

Pomakhina, E., Deneele, D., Gaillot, A.C., Paris, M., Ouvrard, G., 2012. ^{29}Si solid state NMR investigation of pozzolanic reaction occurring in lime treated Ca–bentonite. Cem. Concr. Res. 14, 626–632.

Ramos-Tejada, M.M., Arroyo, F.J., Perea, R., Duran, J.D.G., 2001. Scaling behavior of the rheological properties of montmorillonite suspensions: correlation between interparticle interaction and degree of flocculation. J. Colloid Interface Sci. 235, 251–259.

Shankar, P., Teo, J., Yee-Kwong Leong, Y., Fourie, A., Fahey, M., 2010. Adsorbed phosphate additives for interrogating the nature of interparticles forces in kaolin clay slurries via rheological yield stress. Adv. Powder Technol. 21, 380–385.

Tadros, Th.F., 1996. Correlation of viscoelastic properties of stable and flocculated suspensions with their interparticle interactions. Adv. Colloid Interf. Sci. 68, 97–200.

Tombacz, E., Szekeres, M., 2004. Colloidal behavior of aqueous montmorillonite suspensions: the specific role of pH in the presence of indifferent electrolytes. Appl. Clay Sci. 27, 75–94.

Tombacz, E., Szekeres, M., 2006. Surface charge heterogeneity of kaolinite in aqueous suspension in comparison with montmorillonite. Appl. Clay Sci. 34, 105–124.

Verhasselt, A., 1990. The Nature of the Immediate Reaction of Lime in Treating Soils for Road Construction. American Society for Testing and Materials STP 1095, Philadelphia, pp. 7–17.